# Tunable high-average-power optical parametric oscillators near 2 μm

**BIPLOB NANDY,[1] S. CHAITANYA KUMAR,[1,2,*] J. CANALS CASALS[1,] HANYU YE,[1] AND M. EBRAHIM-ZADEH[1,2,3]**

[1]*ICFO-Institut de Ciencies Fotoniques, The Barcelona Institute of Science and Technology, 08860 Castelldefels (Barcelona), Spain*
[2]*Radiantis, Polígon Camí Ral, 08850 Gavà, Barcelona, Spain*
[3]*Institucio Catalana de Recerca i Estudis Avancats (ICREA), Passeig Lluis Companys 23, 08010 Barcelona, Spain*
**chaitanya.suddapalli@radiantis.com*

**Abstract:** We report on the development of high-average-power nanosecond and picosecond laser sources tunable near 2 μm based on optical parametric oscillators (OPOs) pumped by solid-state Nd:YAG and Yb-fiber lasers at 1.064 μm. By exploiting a 50-mm-long MgO-doped lithium niobate (MgO:PPLN) as the nonlinear crystal and operating the OPO in near-degenerate doubly-resonant configuration with intracavity wavelength selection elements, we have generated tunable high-average-power radiation across 1880-2451 nm in high spectral and spatial beam quality with excellent output stability. In nanosecond operation, pumping with a Q-switched Nd:YAG laser and using an intracavity prism for spectral control, we have generated more than 2 W of average power in pulses of 10 ns duration at 80 kHz repetition rate in narrow linewidth (<3 nm), with $M^2$<2.8, and a passive power stability better than 2.2% rms over 1 hour. In picosecond operation, pumping with a mode-locked Yb-fiber laser and using a diffraction grating as the wavelength selection element, we have generated more than 5 W of average power in pulses of 20 ps at 80 MHz repetition rate in narrow bandwidth (~2.5 nm), with $M^2$<1.8 and a passive power stability better than 1.3% rms over 2 hours. The demonstrated sources represent viable alternatives to $Tm^{3+}$/$Ho^{3+}$-doped solid-state and fiber lasers for the generation of high-power radiation in the ~2 μm spectral range.



OCIS codes: (190.4360) Nonlinear optics, devices; (190.4400) Nonlinear optics, materials; (190.4970) Parametric oscillators and amplifiers.

## 1. Introduction

The spectral region near 2 μm is well known for the high absorption by water and shallow penetration depth of ~0.4 nm, which is useful for various clinical applications [1]. Tunable sources near 2 μm are also of interest due to their utility in applications such as speckle-imaging [2-3], eye-safe differential absorption lidar [4-5], range finding [6], coherent Doppler wind lidar [7], and terahertz (THz) difference-frequency-generation (DFG) [8]. Wavelength generation in the 2-μm region has been achieved using $Ho^{3+}$-doped, $Tm^{3+}$-doped, or $Tm^{3+}$:$Ho^{3+}$ co-doped fiber lasers [9-10], mode-locked Tm:$CaYAlO_4$ (Tm:CYA) laser [11], near-degenerate optical parametric oscillators (OPOs) [12], and, more recently, intracavity OPOs in two-crystal walk-off compensation scheme [13]. Laser sources at ~2 μm and beyond are also necessary for pumping long-wave mid-infrared (mid-IR) OPOs and DFG sources based on non-oxide nonlinear materials such as $ZnGeP_2$, $AgGaS_2$, $AgGaSe_2$ and quasi-phase-matched orientation-patterned gallium arsenide (OP-GaAs) [12,14-17]. Such mid-IR materials offer high nonlinearity and wide transparency into the deep mid-IR, but suffer from two-photon absorption at wavelengths below ~2 μm. Laser sources in such long-wave mid-IR regions are essential for high-resolution spectroscopy, trace gas detection, and environmental sensing in the mid-IR molecular fingerprint region [18]. Currently, commercially available laser sources

in the ~2 μm region are based on $Tm^{3+}/Ho^{3+}$-doped solid-state and fiber lasers, often power-hungry and requiring water-cooling for stable high-power operation, while relying on passive or active acousto-optic Q-switching, typically at fixed repetition rates [19-21].

An alternative approach for efficient and cost-effective generation of tunable laser pulses near 2 μm is to use OPOs pumped by widely available, well-established, and low-cost Nd/Yb-based laser technology at 1.064 μm. This approach has been previously demonstrated in nanosecond OPOs, where by deploying volume Bragg gratings, narrowband radiation at a fixed wavelength near 2 μm has been generated using Q-switched Nd:YAG solid-state pump lasers at 1.064 μm [12,22]. On the other hand, in picosecond operation, the use of diffraction grating has enabled the generation of similarly narrowband radiation at a fixed wavelength near 2 μm in a synchronously-pumped OPO using a mode-locked Yb-fiber laser at 1.064 μm [23]. Here we report high-average-power, high-repetition-rate nanosecond and picosecond OPOs with wavelength tunability near ~2 μm using this approach by deploying Nd/Yb-doped solid-state and fiber lasers at 1064 nm as pump source and MgO-doped lithium niobate (MgO:PPLN) as the nonlinear gain crystal. The demonstrated OPOs operate close to degeneracy, where the output spectrum and bandwidth are controlled by incorporating two different wavelength selection elements, a prism in nanosecond OPO and a diffraction grating in picosecond OPO. The technique allows practical OPO operation at high average powers, with good spectral and spatial beam quality, and high output power stability, over an extended tuning range of 1880-2451 nm, including the degenerate wavelength of 2128 nm.

## 2. High-average-power high-repetition-rate nanosecond OPO near 2 μm

We have developed a high-repetition-rate nanosecond near-degenerate OPO tunable near 2.1 μm by using a Q-switched Nd:YAG laser at 1064 nm as the pump source. The OPO deploys MgO:PPLN as the nonlinear crystal and an intracavity prism for spectral control, output coupling, and output power stabilization. Such a technique has been previously reported in pulsed OPOs in *singly-resonant oscillator* (*SRO*) configuration away from degeneracy [24]. Here, we deploy this approach in a *doubly-resonant oscillator* (*DRO*) operating close to degeneracy, where we demonstrate wavelength tunability across 1880-2128 nm in the signal and 2128-2451 nm in the idler, thus covering ~571 nm across the entire spectral range of 1880-2451 nm, including the degenerate wavelength of 2128 nm. We also show that the deployment of the intracavity prism enables effective control of output spectrum and stabilization of output power in the DRO near or away from degeneracy.

The schematic of the experimental setup for the tunable ~2-μm OPO is shown in Fig. 1. The OPO is pumped by a high-repetition-rate Q-switched Nd:YAG laser (Bright Solutions, *Sol*) delivering up to ~30 W of average power in linear polarization with a variable repetition rate from 20 to 100 kHz. The laser operates at a central wavelength of 1064 nm with a full-width at half-maximum (FWHM) bandwidth of ~0.2 nm and exhibits spectral jitter of ~1 nm over 30 s. For pumping the OPO, we chose a fixed repetition rate of 80 kHz in order to avoid any optical damage to the MgO:PPLN crystal caused by increasing pulse energy fluence at lower repetition rates. At 80 kHz repetition rate, the pump pulses have a FWHM duration of ~23 ns. Also shown in the inset of Fig. 1 is a laboratory photograph of the OPO incorporating an uncoated intracavity prism (P) for spectral control and output coupling. The pump power is adjusted by the combination of a half-wave plate (HWP) and a polarizing beam-splitter (PBS). The pump beam polarization is adjusted for optimum phase-matching in the MgO:PPLN crystal under type-0 (*ee*→*e*) interaction. After preparation of the pump beam for systematic input power control and polarization, it is focused to a waist radius of $w_0$~300 μm at the center of the crystal, which is 50-mm-long and incorporates a single grating period of $\Lambda$=32.16 μm. The crystal end-faces are antireflection (AR)-coated for high transmission ($R$<0.5%) at 1064 nm and over 2050-2150 nm. The crystal is mounted in an oven providing temperature control from 32 to 100 °C with a stability of 0.1 °C, thus covering OPO operation through wavelength degeneracy.

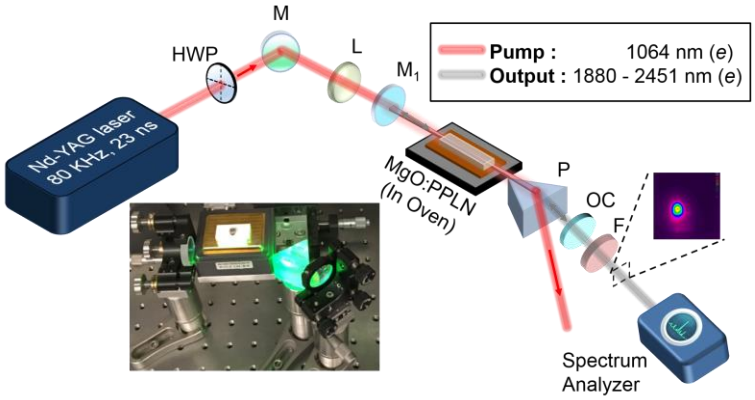


**Fig. 1.** Schematic of the experimental setup for the intra-cavity prism-coupled tunable 2 μm source. HWP, half-wave plate; M, mirrors; L, lens; $M_1$, input plane mirror; P, TF3 prism; OC, output coupler; F, filter. Inset: Visualization of the actual setup.

The OPO is configured in a linear standing-wave cavity with an input plane mirror, $M_1$, which is highly transmitting for the pump ($T$>90%) at 1064 nm and highly reflecting ($R$>99%) over 1800-2150 nm, resulting in OPO operation in DRO configuration near degeneracy. The plane output coupler (OC) has varying transmission ($T$~60-90%) over the OPO tuning range. Owing to the large parametric gain bandwidth near degeneracy, an uncoated TF3-glass prism (apex angle: 60.8°) is incorporated within the OPO cavity for wavelength selection, linewidth control, and spectral tuning around ~2 μm. The TF3 glass has a refractive index of ~1.7 and high transmittance ($T$>94%) in the 2 μm spectral region. The total single-pass optical path length of the OPO cavity is ~165 mm, allowing ~21 round-trips of the signal and idler parametric waves over the ~23 ns duration of the pump pulse. The undepleted pump exits the cavity through the prism, P, at a different angle from the signal and idler waves, and is dumped onto a beam block, ensuring single-pass pumping of the prism-coupled OPO. A long-pass filter, F, with >90% transmission above 1.65 μm is used to extract the total output power (signal plus idler) from the pump. A second filter with high transmission ($T$>95%) over 1300-2000 nm is used to extract signal wavelengths up to ~2 μm, beyond which the signal and idler begin to approach degeneracy.

We initially investigated the tuning characteristics of the OPO. Wavelength tuning in the prism-coupled OPO was achieved by varying the crystal temperature. We first studied temperature tuning of the OPO together with the total average output power variation across the tuning range for a fixed prism incidence angle of ~60° in the cavity. By varying the temperature of the MgO:PPLN crystal over 32-81 °C, we were able to tune the generated signal across 1880-2128 nm, together with the corresponding idler across 2451-2128 nm, resulting in a total (signal plus idler) tuning over 571 nm. The results are shown in Fig. 2, where the solid circles represent the measured signal wavelengths, while the hollow circles correspond to the total average output power from the OPO as a function of crystal temperature. The measurements were performed for a fixed input average pump power of 17.8 W (corresponding to a pump pulse energy of 0.22 mJ) and the power data are not corrected for the transmission loss (~10%) of the filter, F. As can be seen, the total average output power from the OPO remains nearly constant at ~2 W over the signal wavelength range of 1898-2090 nm (corresponding to a crystal temperature of 40-70 °C), with the total OPO output power (pulse energy) increasing from 1.45 W (18.1 μJ) to 2.1 W (26.3 μJ) as the

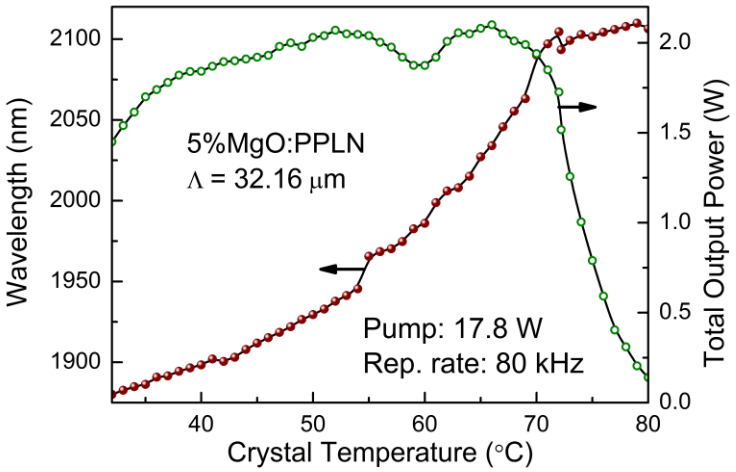


**Fig. 2.** The signal wavelength tuning range and total output power generated from the prism-coupled nanosecond OPO. The solid curves are guide to the eye.

crystal temperature is increased from 32 °C to 66 °C. However, further increasing the temperature up to 81 °C results in the decline in output power down to 0.14 W (1.75 μJ), due to the broadening of signal bandwidth towards degeneracy. As a result of the dispersion through the intracavity prism, an increasingly smaller fraction of total signal spectrum can be supported by the cavity as the OPO is tuned towards degeneracy, thus leading to a sharp decline in the output power. The recorded OPO average output power (pulse energy) of ~2 W (25 μJ) at 55 °C corresponds to a measured signal power (pulse energy) of ~0.9 W (11.3 μJ) at 1965 nm and an estimated idler power (pulse energy) of 1.1 W (14 μJ) at 2320 nm. The average power of 2.1 W from the OPO represents a single-pass conversion efficiency of 11.8% and photon conversion efficiency of 10.7% and 13% for the signal and idler, respectively. By deploying an AR-coated intracavity prism for wavelength selection, further improvements in OPO output power and efficiency are expected. Figure 3 shows the phase-matched temperature tuning of the OPO together with the theoretical calculation. The

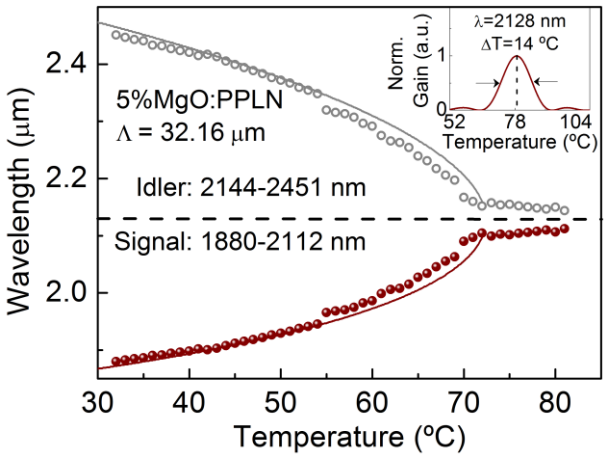


**Fig. 3.** Wavelength tuning of the OPO. The filled and hollow circles represent the experimental data, while the solid curve is the calculated tuning range. Inset: Temperature acceptance bandwidth for degenerate operation at 2128 nm.

measurements were performed using an InGaAs spectrometer (StellarNet RED-Wave NIRX-SR-100 T2 BW) with a resolution of about 15 nm. The solid circles represent the experimentally measured signal wavelengths, while the hollow circles are the corresponding idler wavelengths estimated from energy conservation. The solid curves are the theoretical calculations using the relevant Sellmeier equations for MgO:PPLN [25]. The discrepancy between the experimental data and theoretical calculations is attributed to the limited resolution of the spectrometer. Further, the relatively flat wavelength response as a function of the temperature close to degeneracy is due to the broad temperature acceptance bandwidth of ΔT=14 °C at a phase-matching temperature of 78 °C, as shown in the inset of Fig. 3 enabling degenerate operation of the OPO around 2128 nm.

We also recorded the signal spectrum over the entire temperature tuning range of the prism-coupled OPO at fixed prism incidence angle of ~60°. The measurements were performed using the same InGaAs spectrometer used for temperature tuning measurements, with a resolution of 15 nm in the ~2 μm region. The results are shown in Fig. 4(a), confirming signal tuning from 1880 nm to degeneracy at 2128 nm, for a change in the MgO:PPLN crystal temperature from 32 °C to 78.5 °C. The spectral stability of the degenerate output at the temperature of 78.5 °C was also recorded over 1 hour, and the center wavelength was found to be stable to within ±2 nm with 0.1% rms, as shown in Fig. 4(b). The corresponding FWHM bandwidth at degeneracy was also measured to be stable within ±3 nm with 6.2% rms over the same period, as shown in Fig. 4(c). In these experiments, the measurement accuracy was constrained by the limited resolution of the spectrometer.

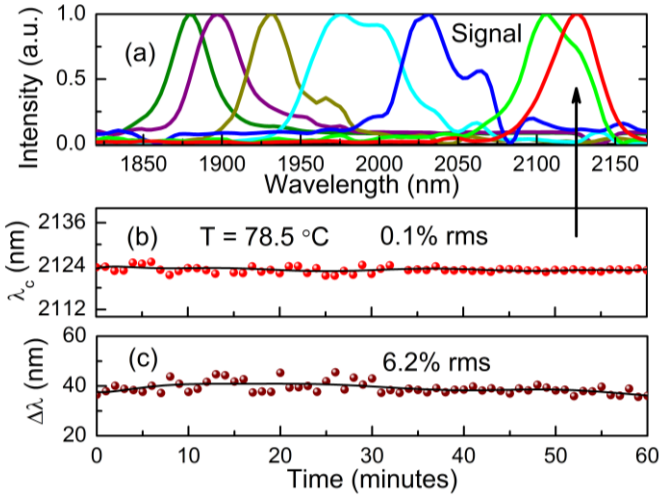


**Fig. 4.** (a) Signal spectrum over the entire tuning range of the OPO. (b) Spectral stability over 1 hour measured near degeneracy. (c) Spectral bandwidth stability over 1 hour measured near degeneracy.

In order to determine the spectral quality of the prism-coupled OPO with higher accuracy, we further constructed a home-made grating spectrometer, and performed spectral measurements close to wavelength degeneracy. The device comprised of a 420 lines/mm diffraction grating mounted on a rotation stage with 0.01° angular precision and a sensitive power meter. The degenerate OPO output at a crystal temperature of 78.5 °C was filtered using a 1.65 μm cut-on filter and collimated using a $f$=150 mm lens before entering the spectrometer. The spectral components in the OPO output are separated upon reflection from the grating, and are then focused onto a slit and recorded using a power meter. For this arrangement, we can calculate the first-order diffraction angle by using the grating equation,

$$d \times [sin(a - \Delta x) + sin(b + \Delta x)] = m \times \lambda \qquad (1)$$

where $d$ is the spacing between two adjacent grooves on the diffraction grating, $a$ is the angle of incidence, $b$ is the diffraction angle, $\Delta x$ is the change in the incidence angle corresponding to the rotation of the diffraction grating, $m$ is diffraction order, and $\lambda$ is the central wavelength of the incident beam. For our device, $d$=2.38 μm, $a$=40.22°, λ=2.128 μm, $m$=1, and $b$ is calculated to be 14.38°. Using this equation, we can ensure the calibration of the grating spectrometer. By changing $\Delta x$, using the rotation stage on which the grating is mounted, and measuring the power, the spectral intensity as a function of wavelength is recorded. The measured FWHM spectral bandwidth is limited by the resolving power of the diffraction grating, which is given by

$$R = m \times N = \lambda/\Delta\lambda \qquad (2)$$

where $m$ is the diffraction order, $N$ is the total number of grooves illuminated on the surface of the grating from the incident laser, and Δλ is the resolution limit. The resolving power, $R$, is a measure of the ability of grating to separate adjacent spectral lines of average wavelength, λ. In our case, the measured input beam diameter is ~2.5 mm, resulting in a calculated beam size of 3.3 mm on the grating surface, for an incidence angle of α=40.22°, covering 1386 grooves. Considering λ=2128 nm, the limit of resolution is calculated to be Δλ=1.5 nm, while the wavelength scanning step is estimated to be 0.1 nm for a minimum angular increment of 0.01° on the grating rotation stage.

By using the home-built spectrometer, we further studied the OPO output spectrum across the tuning range near degeneracy by varying the crystal temperature from 71 °C to 78.5 °C, corresponding to the degenerate wavelength of ~2128 nm. The results are shown in Fig. 5, where Δ represents the separation between the signal and idler peaks. It can be seen that,

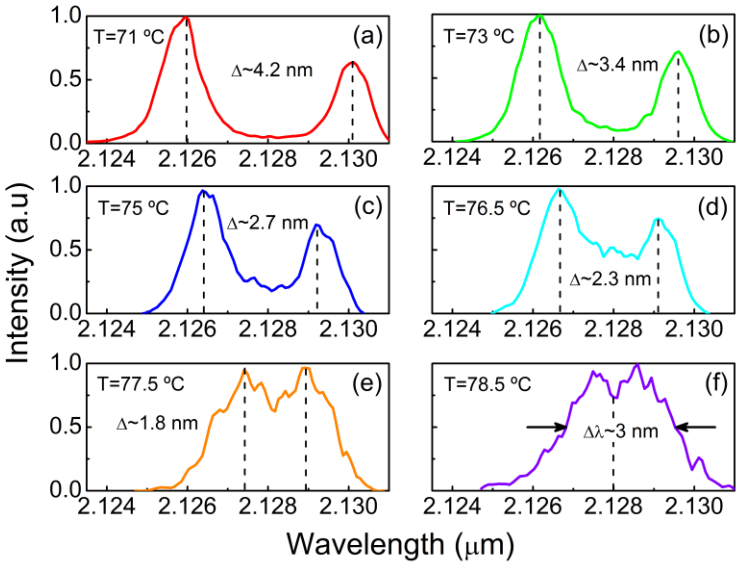


**Fig. 5.** Spectral bandwidth measurements of the OPO output using the home-built grating spectrometer**.** (a) Spectrum at 71 °C with peak separation (Δ) of 4.2 nm. (b) Spectrum at 73 °C with Δ~3.4 nm. **(c)** Spectrum at 75 °C with Δ~2.7 nm. (d) Spectrum at 76.5 °C with Δ~2.3 nm. (e) Spectrum at 77.5 °C with Δ~1.8 nm. (f) Spectrum at degeneracy temperature of 78.5 °C with center wavelength at 2128 nm and FWHM of ~3 nm.

away from degeneracy there are two distinct signal and idler peaks, while increasing the crystal temperature the two peaks begin to merge, finally resulting in a composite spectrum centered at the degenerate wavelength of 2128 nm. It is also evident from Fig. 5(a)-(e) that the signal and idler peak wavelength separation gradually decreases from 4.2 nm at 71 °C to 1.8 nm at 77.5 °C. The peaks finally merge into a single spectrum at a crystal temperature of 78.5 °C at degeneracy with center wavelength at 2128 nm and FWHM bandwidth of ~3 nm, as shown in Fig. 5(f).

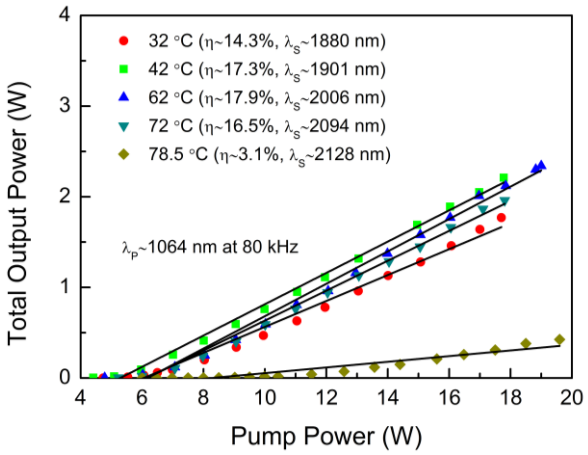


**Fig. 6.** Output power scaling of the prism-coupled MgO:PPLN OPO at various temperatures.

We studied power scaling of the prism-coupled OPO at various crystal temperatures, and the corresponding signal wavelengths, by recording the total (signal plus idler) output power as a function of input pump power. The results are shown in Fig. 6. The measurements were performed for an available average pump power of 17.8 W at 80 kHz pulse repetition rate. For each crystal temperature, we measured the slope efficiencies as well as pulse duration at maximum output power. The measurements resulted in typical slope efficiencies of ~14% to 18% for crystal temperatures ranging from 32 °C to 72 °C, with the lowest slope efficiency of ~3% obtained at 78.5 °C. The corresponding maximum total average power and output signal pulse duration at different wavelengths are shown in Fig. 7. The OPO average output power varies from 1.45 W to 2.1 W over the signal wavelength range of 1880-2110 nm, with the power remaining >1.5 W across nearly the full range and the highest power at 2034 nm.

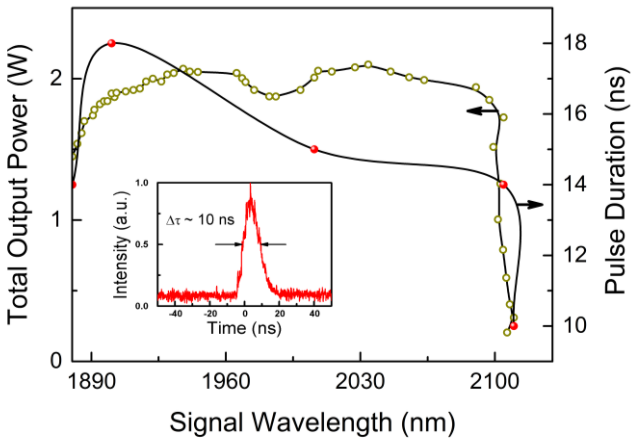


**Fig. 7.** Maximum average output power and output pulse duration at different signal wavelengths. Inset: Pulse duration measurement at degeneracy.

The FWHM output signal pulse duration, measured using a fast photodetector with a rise-time <200 ps in the OPO wavelength range, was recorded to vary over ~14-18 ns over the same wavelength range. At the degenerate wavelength of 2128 nm, the OPO delivers an average power of 400 mW, with corresponding pulse duration of ~10 ns, as shown in the inset of Fig. 7. We attribute the shortening of the pulse duration at degeneracy to the increase in the OPO buildup time due to the rise in threshold caused by spectral broadening, which is also accompanied by the decline in output power, as described previously and observed in Fig. 2 and Fig. 7.

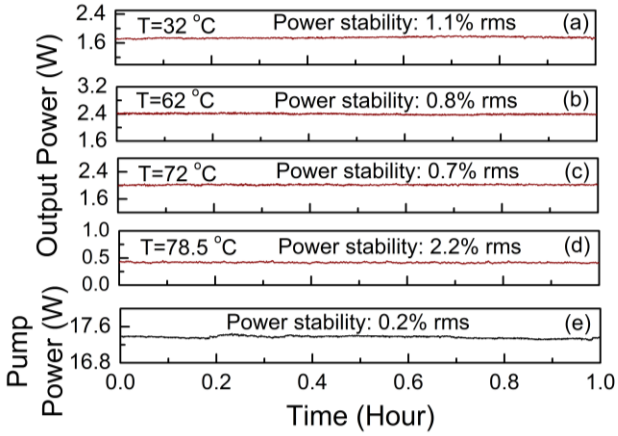


**Fig. 8.** (a)-(d) Measurements of power stability for the OPO at different crystal temperatures, corresponding to different output wavelengths, and (e) the pump beam over 1 hour.

We also performed measurements of output power stability from the prism-coupled OPO at different MgO:PPLN crystal temperatures, corresponding to different wavelengths near 2 μm. The output power was recorded over 1 hour, with the results shown in Fig. 8 (a)-(d). As can be seen, the OPO exhibits a passive long-term power stability ranging 0.7% rms to 1.1% rms over the crystal temperature range of 32 °C to 72 °C, with a stability of 2.2% rms at 78.5 °C. Figure 8 (e) shows the power stability of the Nd:YAG pump laser, measuring 0.2% rms over the same period.

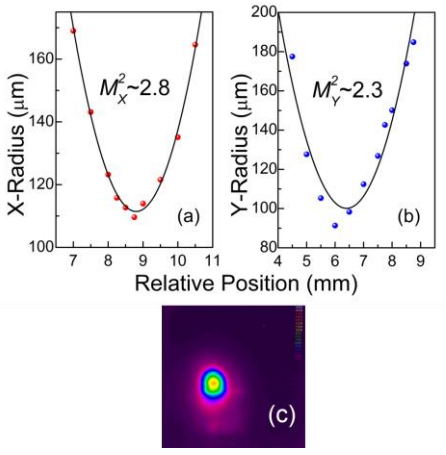


**Fig. 9.** (a)-(b) Measurement of $M^2$ beam quality of the OPO output at the degenerate wavelength of 2128 nm along X- and Y-axis. (c) Spatial beam profile of the OPO output at degeneracy.

We further recorded the spatial quality of the output beam from the prism-coupled OPO at the degenerate wavelength of 2128 nm. Using a focusing lens of focal length, $f$=50 mm, and a scanning beam profiler, we measured the $M^2$-value of the output beam at 78.5 °C, resulting in $M^2_x$ <2.8 and $M^2_y$ <2.3, as shown in Fig. 9(a)-(b). The degenerate output beam was also observed to exhibit high spatial quality with single-mode Gaussian distribution, as presented in the inset of Fig. 9(c).

Finally, we performed a detailed comparison of performance of the prism-cavity OPO with a standard free-running OPO without the prism, in a cavity formed by the same plane high reflector and OC as in Fig. 1, separated by 78 mm, and operating under the same conditions. Both the OPOs were optimized to generate maximum power together with narrow spectral bandwidth. The spectrum of the standard nanosecond OPO using plane mirrors, operating close to degeneracy, measured using a commercial spectrometer, together with the spectrum from the nanosecond OPO with intracavity prism for spectral control is shown in Fig. 10. Due to the limited resolution of the commercial spectrometer, we used a diffraction grating-based home-made spectrometer to measure the spectrum from the prism-cavity nanosecond OPO. As evident the spectral quality of the output is significantly improved with bandwidth reduced from 50 nm (centered at 2092 nm) in the standard plane-mirror cavity to 3 nm (centered at 2128 nm) in the prism cavity.

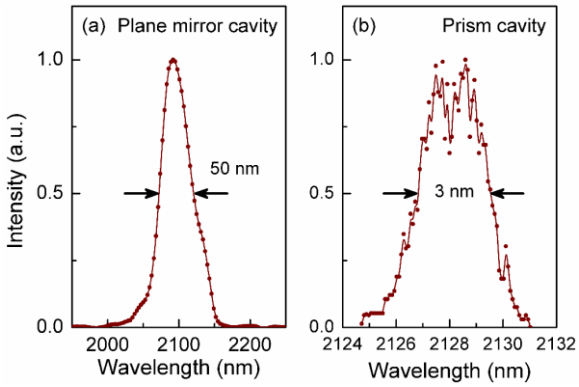


**Fig. 10.** Output spectrum from the nanosecond OPO using (a) conventional plane-mirror cavity with no frequency selection elements, and (b) prism cavity

**Table 1. Comparison of the performance characteristics of the plane mirror nanosecond OPO with prism cavity.**

| Nanosecond 2.1 μm OPO<br>Parameter | Plane Mirror Cavity | Prism Cavity |
|---|---|---|
| Wavelength (nm) | 2092 | 2128 |
| Spectral bandwidth (nm) | 50 | 3 |
| Output power (W) | 4.3 | 0.4 |
| Slope efficiency (%) | 39 | 3.1 |
| Power stability over 1 hour (% rms) | 0.61 | 2.2 |
| Spatial mode | $TEM_{00}$ | $TEM_{00}$ |
| Beam quality | --- | $M^2$<2.8 |
| Repetition rate (kHz) | 80 | 80 |

The main performance characteristics of the prism-cavity nanosecond OPO are compared with that of the plane mirror cavity in Table 1. It is clear that the prism-cavity OPO surpasses the performance of conventional plane-mirror OPO in most respects, except for output power and efficiency. However, with further design improvements including the use of an AR-coated prism as well as optimization of output coupling, we expect substantial enhancement in output power and efficiency from the prism-cavity OPO.

## 3. High-average-power high-repetition-rate picosecond OPO near 2 μm

We have also developed a stable high-average-power high-repetition-rate picosecond source at ~2.1 μm in linear polarization. This source is similarly based on a degenerate OPO in DRO configuration, but deploys a diffraction grating as the frequency selective element for spectral control and output power stabilization. The approach similarly overcomes the output power and spectral instabilities typical of OPOs in DRO configuration. Using this technique, our ~2.1 μm picosecond source provides ~5.25 W of average power with high stability, at ~36% conversion efficiency at ~80 MHz repetition rate. The output exhibits a long-term power stability better than 1.3% rms over 2 hours, high spatial quality with $M^2$<1.8, and narrow bandwidth of Δλ~2.9 nm. We further reduce the spectral bandwidth down to ~2.5 nm by using an intracavity telescope in one arm of the OPO cavity.

The schematic of the experimental setup for the ~2.1 μm is shown in Fig. 11. The OPO is pumped by an Yb-fiber laser delivering 15 W of average power at a central wavelength of 1064 nm with a FWHM spectral bandwidth of $\Delta\lambda_p$~1 nm, in pulses of ~20 ps duration at a ~80 MHz repetition rate. A combination of a half-wave plate (HWP) and a polarizing beam-splitter (PBS) is used for systematic control the laser pump power, while a second half-wave plate is used to control the linear input polarization for optimum phase-matching in the nonlinear crystal. The pump beam is focused to a waist radius of $w_{0P}$~130 μm, corresponding to a focusing parameter of ξ~0.23, in a 50-mm-long 5%MgO:PPLN crystal incorporating a single grating period of Λ=32.16 μm for type-0 (*ee*→*e*) quasi-phase-matching, identical to that used for the nanosecond OPO in Section 2. The crystal end-faces are similarly AR-coated for high transmission ($R$<0.5%) at 1064 nm and over 2050-2150 nm. The crystal is mounted in an oven providing temperature control from 32 to 100 °C with a stability of 0.1 °C, thus covering OPO operation through wavelength degeneracy. The OPO is configured in a standing-wave X-cavity formed by two plano-concave mirrors, $M_1$-$M_2$, with radius of

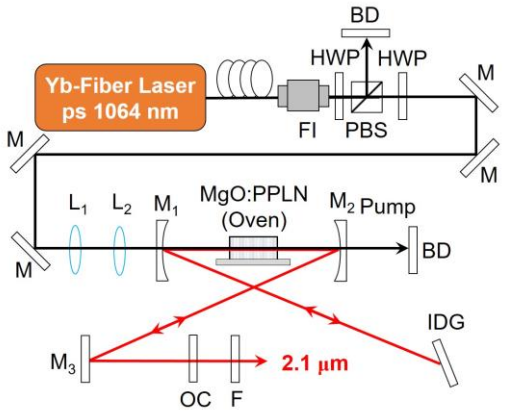


**Fig. 11.** Schematic of the experimental setup for the ~2.1 μm source pumped by a Yb-based fiber laser at 1064 nm. FI, faraday isolator; HWP, half-waveplate; PBS, polarizing beam splitter; BD, beam dumper; M, mirrors, L, lenses, IDG, intracavity diffraction grating, OC, output coupler; F, filter.

curvature, $r$=200 mm, a plane mirror, $M_3$, an output coupler (OC), and an aluminium intracavity diffraction grating (IDG). All mirrors are highly transmitting ($R$<90%) for the pump at 1064 nm and highly reflecting ($R$>99%) over 1800-2150 nm, resulting in DRO operation close to degeneracy. The plane OC has partial transmission ($T$~87%) at 2.1 μm. The total round-trip optical length of the OPO cavity is ~3.78 m, corresponding to a repetition rate of ~80 MHz, ensuring synchronization with the pump laser repetition rate. The IDG is configured in a Littrow configuration, where the incident angle is equal to the diffracted angle, and the beam is thus reflected back and can resonate in the cavity. A Ge filter (F) is used to separate the OPO output beam at ~2.1 μm from residual pump after the OC.

In order to generate an output wavelength at ~2.1 μm using a pump source at 1064 nm, the temperature of the MgO:PPLN crystal with a grating period of Λ=32.16 μm has to be set to T~72 °C, to allow phase-matching near degeneracy. Under this condition, both signal and idler waves can oscillate in the DRO cavity, which combined with increased parametric gain close to degeneracy, result in major increase in intracavity power, and thus substantially lower threshold compared to singly-resonant oscillator configuration [26]. Therefore, significantly lower peak pump intensities can be used to drive the DRO, and thus in our experiment the beam waist in the center of the crystal was increased up to $w_0$~130 μm. The high nonlinearity of MgO:PPLN, together with the long interaction length and the high peak powers in picosecond regime, enable high conversion efficiencies together with high output power from the picosecond OPO, even in the presence of large output coupling losses. As such, an output coupling as large as $T$~87% was used for the DRO to maximize the generated average power and extraction efficiency. In addition, operating close to degeneracy, the OPO provides large parametric gain with broad bandwidth and low temporal walk-off [26]. For a 50-mm-long MgO:PPLN crystal with a grating period of Λ=32.16 μm at a temperature of T~72 °C, the parametric gain bandwidth at ~2.1 μm is calculated to be Δλ~144 nm for pumping at 1064 nm, as shown in Fig. 12(a). The group velocity mismatch (GVM) between the pump and signal, and the corresponding group velocity dispersion (GVD), as a function of the signal wavelength is also shown in Fig. 12(b). At the degenerate wavelength of 2128 nm, the GVM is calculated to be ~113 fs/mm, whereas GVD is approximately –68 fs$^2$/mm.

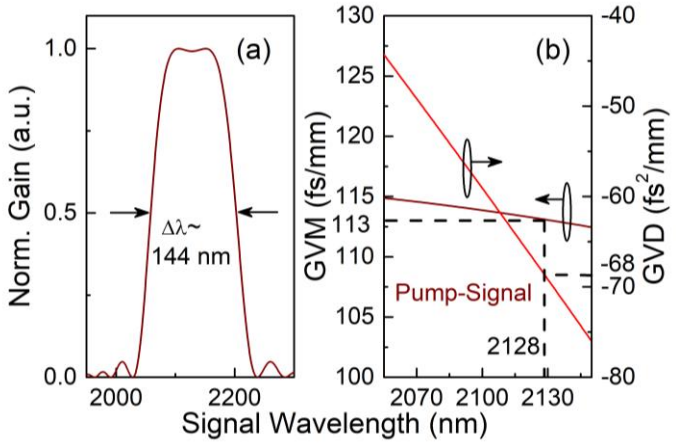


**Fig. 12.** (a) Parametric gain bandwidth of the OPO at degeneracy. (b) GVM between the pump and the signal and the corresponding GVD as a function of the signal wavelength.

We first performed spectral characterization of the OPO output at a crystal temperature of T=71 °C using a 400 lines/mm IDG at a blaze angle of 25.2°. The result is shown in Fig. 13(a) where a central wavelength at λ=2128 nm with a FWHM spectral bandwidth of Δλ~2.9 nm was recorded. The measurement was performed using a home-made spectrometer. The spectral bandwidth of the output from the OPO incorporating the IDG is given by [27]

$$\Delta\lambda_{estimated}=\frac{\sqrt{ln(2)\lambda^2}}{\pi w_0 tan(\theta)} \qquad (3)$$

where $w_0$ is the beam radius on the IDG and θ is the incidence angle of the resonant beam on the IDG in Littrow configuration, which depends on the wavelength and the grove spacing.

The calculated FWHM spectral bandwidth as a function of the beam diameter on the IDG with 400 lines/mm is shown in Fig. 13(b), indicating a FWHM spectral bandwidth of Δλ~2.3 nm and Δλ~1.15 nm for a beam diameter of $2w_0$~2.2 mm and $2w_0$~4.4 mm, respectively on the IDG. Also shown in the inset of Fig. 13(b) is the experimentally measured beam diameter of 2 mm at the position of the IDG, resulting in a calculated beam diamter of $2w_0$~2.2 mm on the surface of the IDG.

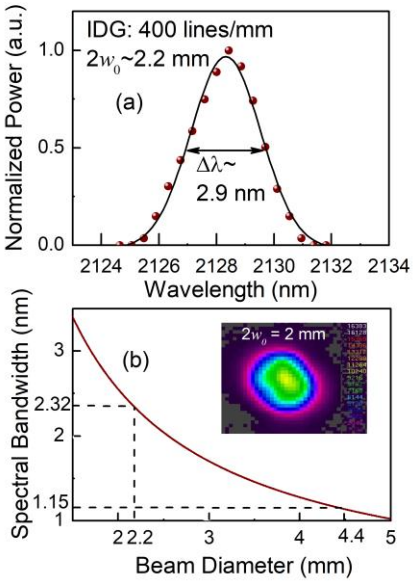


**Fig. 13.** (a) Spectral characterization of the output beam from the OPO using a 400 lines/mm IDG at blaze angle of 25.2°. (b) Calculated FWHM spectral bandwidth as a function of the beam diameter on the IDG with 400 lines/mm. Inset: Measured beam profile in the diffraction grating.

To further reduce the output spectral bandwidth at the degenerate wavelength of 2128 nm, we increased the beam diamter to $2w_0$~4.4 mm on the grating by using a telescope with magnification of 2 in one of the arms of the OPO cavity. However, the FWHM spectral bandwidth of the output from the OPO is measured to be >2.5 nm, still limited by the resolution of the spectrometer. Hence, using a spectrometer with higher resolution, narrower spectral bandwidth is expected. Considering 20 ps output pulses from the OPO with a expected FWHM bandwidth of Δλ~1.15 nm, we obtain a time-bandwidth product of $\Delta\tau\Delta\nu$~1.52 in the absence of dispersion compesation, This indicates operation of the ~2.1 μm picoscoend OPO near the transform limit ($\Delta\tau\Delta\nu$~0.44), despite the large time-bandwidth product of $\Delta\tau\Delta\nu$~5.3 for the pump laser.

In order to characterize the output power characteristics of the ~2.1 μm picosecond OPO, we performed power scaling measurements at crystal temperature of 71 °C, corresponding to a signal wavelength of 2128 nm, and with the OC extracting ~87% of the intracavity power. The result is shown in Fig. 14(a), where it can be seen that up to 5.25 W of average power was generated for an input pump power of 15 W, without considering the transmission loss of the Ge filter estimated as ~8% at 2.1 μm. It can be also seen that the generated power increase linearly with input power at a slope efficiency of ~43%, with a maximum extraction efficiency

of ~36% and external photon conversion efficiency of ~60% at full pump power of 15 W. The pump depletion is ~60% near the maximum input power, while the OPO threshold is measured to be ~2.6 W. We also recorded the long-term stability of output power, with OPO generating an average power of ~5 W at 2.1 μm. The result is presented in Fig. 14(b),

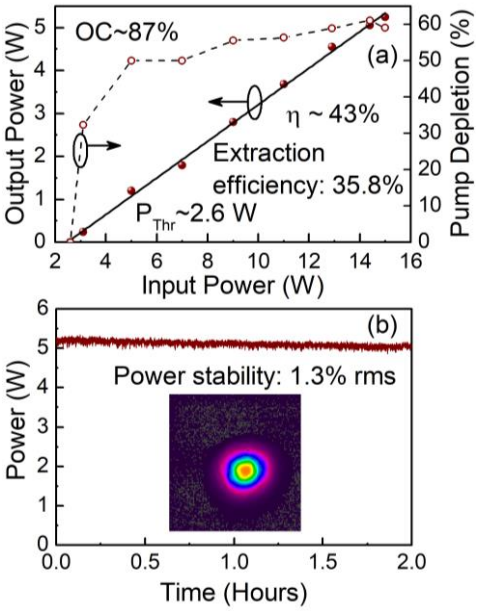


**Fig. 14.** (a) Simultaneously measured output power and pump depletion as a function of the pump power for the picosecond OPO, and (b) long-term power stability of the output from the degenerate OPO operating at 2.1 μm. Inset: spatial beam distribution of the OPO output at 2128 nm.

where a passive power stability of 1.3% rms over 2 hours. The stability of the pump laser was recorded to be <0.3% rms over the same period of time. The spatial profile of the output beam measured at a distance of ~75 mm from the cavity is shown in the inset of Fig. 14(b) exhibiting single-peak Gaussian spatial intensity distribution with $TEM_{00}$ mode profile with circularity ~90%.

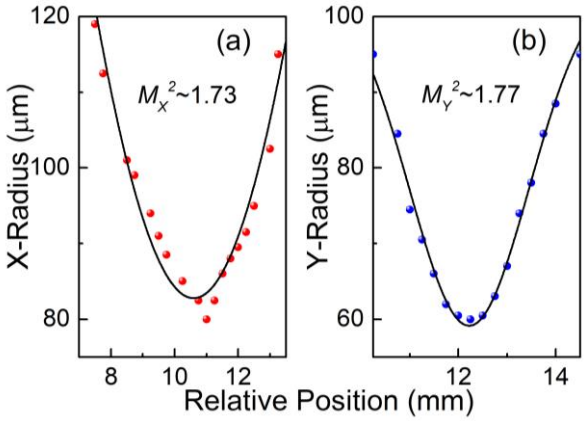


**Fig. 15.** $M^2$ measurement of the output beam at degeneracy along (a) X-axis and (b) Y-axis.

We performed further measurements of spatial beam quality at the degenerate wavelength of 2128 nm, with the OPO delivering output power ~4.5 W. Using a lens with focal length,

$f$=50 mm, and a scanning beam profiler, we recorded the beam radius across the Rayleigh range and estimated the $M^2$ values, resulting in $M_x^2$<1.73 and $M_y^2$<1.77, as shown in Fig. 15 (a-b).

We also investigated cavity-delay tuning of the OPO for an input pump power of 13 W, at a temperature of ~71 °C, corresponding to the degenerate wavelength of 2128 nm. The output power as a function of cavity detuning is shown in Fig. 16. The cavity detuning is normalized to zero for the maximum power at the center of the detuning range. As the cavity length detuning is adjusted from –4.5 mm to +4.9 mm, the output power remains well above 3 W over the entire range with multiple peaks and a maximum of 4.6 W at zero detuning. This tolerance of the OPO operation, inspite of the large cavity detuning of ~10 mm is enabled by the low GVM at degeneracy, resulting in a temporal walk-off of ~5.6 ps, which is ~4 times lower than the ~20 ps pump and signal pulse durations. Further, the temporal walk-off-limited intraction length is estimated to be ~177 mm, which is ~3.5 times greater than the length of the MgO:PPLN crystal used in this experiment. The power peaks at –3.4 mm and +3.3 mm correspond to signal beams at slightly different wavelengths withinin the selectivity band of the diffraction grating that have better temporal overlap with the pump pulses. However, we could not measure this wavelength shift, due to the limited resolution of our spectrometer. If we do not consider these two peaks, a slightly asymmetric power behaviour is observed with more sensitivity in the positive detuning, as also observed previously [27]. In our case, we do not have a large asymmetry because of the similar group velocity of the pump and the resonant signal in the cavity, $v_{gs}$~1.38×10$^8$ and $v_{gp}$~1.36×10$^8$, which mitigates the nonlinear pulse-shaping effects.

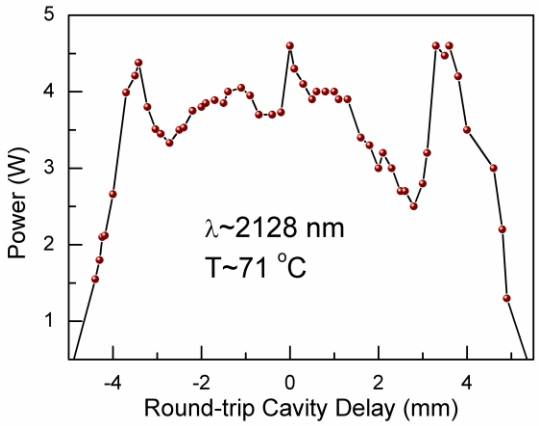


**Fig. 16.** Cavity-delay tuning of the OPO for an input pump power of 13 W at degeneracy.

We futher studied the wavelength tunability of the picosceond OPO around the ~2.1 μm output by rotating the IDG with 400 lines/mm. When operating in Littrow configuration, for an incidence angle of θ on the IDG, only the associated wavelength, λ, is exactly reflected on itself, allowing the OPO oscillation according to equation

$$\lambda = 2d \sin(\theta) \qquad (4)$$

where λ is the reflected wavelength at the angle θ=α=β, and $d$ is the spacing between two adjacent grooves. The measured spectra at different IDG angles, expressed as angle deviation with respect to the blaze angle of 25.2° of the IDG, are shown in Fig. 17. By decreasing the angle deviation, the resonant central wavelength in the cavity is also reduced. Using this method, we were able to tune the OPO near ~2.1 μm, generating different spectra for different IDG angles. The output spectra, measured using a commercial spectrometer (StellarNet RED-Wave NIRX-SR-100 T2 BW) with resolution ~15 nm, are shown in Fig. 17(a). The spectrum

with central wavelength at 2128 nm was obtained for a blaze angle at 25.2° or blaze angle deviation of 0°. However, with progressive decrease in the IDG angle, the resonant wavelength in the OPO cavity drops, reaching a minimum wavelength of 2030 nm for an IDG angle at –1.2° deviation from the blaze angle.

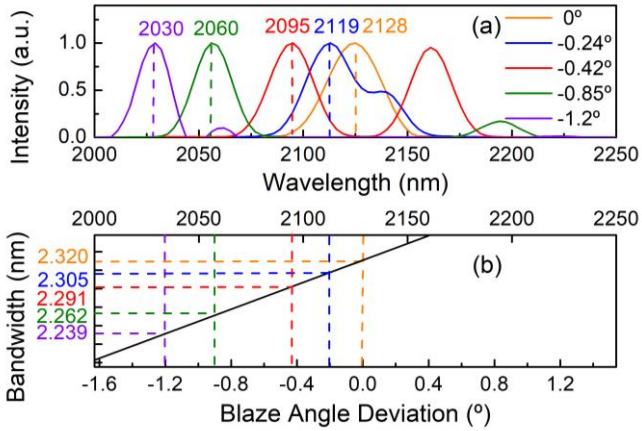


**Fig. 17.** Spectrum of the resonating signal from the picosecond OPO at different IDG angles. and, (b) estimated spectral bandwidth selectivity as a function of the blaze angle deviation.

We also calculated the FWHM spectral bandwidth of the output spectra as a function of the resonant wavelength in the cavity and the corresponding IDG angle, as shown in Fig. 17(b). The result confirms that in the case of the double-peak spectrum generated for an angle deviation of –0.42°, the idler wavelength cannot be resonant in the cavity when we operate away from degeneracy because it is out from the spectral selectivity band imposed by the IDG. Hence, this second peak is the residual idler generated from the resonating signal and the pump beam that has not been completely extracted from the cavity.

Similarly, we performed detailed comparison of performance of the synchronously-pumped picosecond OPO operating near degeneracy using intracavity IDG with an OPO using a conventional plane mirror. The spectral characteristics for the two OPOs are presented in Fig. 18, where the measured output spectra in both cases are compared. Again, it is clear that substantial bandwidth reduction from 115 nm (centred at ~2040 nm) in the case of standard plane-mirror OPO to 2.9 nm (centred at 2128 nm) in the OPO with IDG is obtained.

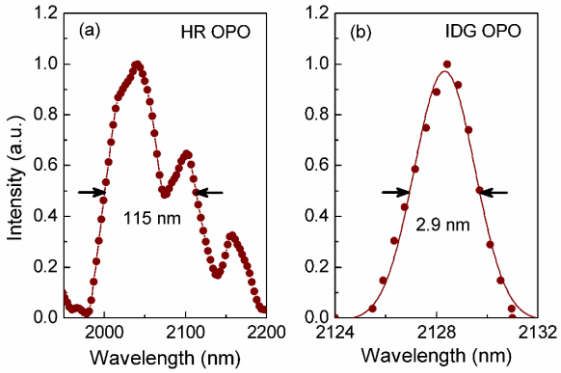


**Fig. 18.** Output spectrum from the synchronously-pumped picosecond OPO using (a) plane mirror cavity and (b) intracavity diffraction grating in Littrow configuration for spectral control.

The main performance characteristics of the picosecond OPO in both configurations are presented in Table. 2. As can be seen, the picosecond synchronously-pumped OPO with IDG

for spectral control delivers superior performance to standard OPO using plane mirror in almost all respects, providing stable, high power, linearly polarized 2.1 μm picosecond pulses at 80 MHz repetition rate, with well-controlled spectrum and high spatial beam quality.

**Table 2. Comparison of the performance characteristics of the plane mirror picosecond OPO with IDG cavity.**

| Picosecond 2.1 μm OPO<br>Parameter | Plane Mirror Cavity | IDG Cavity |
|---|---|---|
| Wavelength (nm) | ~2040 | ~2128 |
| Spectral bandwidth (nm) | ~115 | 2.9 |
| Output power (W) | 4.3 | 5.25 |
| Power stability over 2 hours (% rms) | ~1 | 1.3 |
| Pulse-to-pulse stability over 2 μs (%rms) | 2.6 | 3.4 |
| Round-trip cavity delay tolerance (mm) | 24 | 10 |
| Spatial mode | $TEM_{00}$ | $TEM_{00}$ |
| Beam quality | $M^2$<2.3 | $M^2$<1.8 |
| Repetition rate (MHz) | 80 | 80 |

## 4. Conclusions

In conclusion, we have demonstrated stable and practical operation of pulsed nanosecond and picosecond OPOs near 2 μm by exploiting Nd/Yb solid-state and fiber lasers at 1064 nm as the pump source and a 50-mm-long MgO:PPLN crystal incorporating a single grating period of Λ=32.16 μm as the nonlinear gain material. Operating the OPOs in DRO configuration close to degeneracy, and deploying an intracavity prism and a diffraction grating for spectral and bandwidth control, we have generated high-average-power high-repetition-rate radiation tunable across the 1880-2451 nm spectral range. In both operating domains, the use of intracavity wavelength selection elements has enabled high spectral quality with narrow bandwidth together with high spatial quality and excellent output stability. In nanosecond operation, we have generated up to 2.1 W of average power in pulses of 10-20 ns duration at 80 kHz repetition rate with a FWHM spectral bandwidth down to ~3 nm, in high beam quality with $M^2$<2.8, with passive power stability as high as 0.7% rms over 1 hour. In picosecond operation, we have achieved up to 5.25 W of average power at 80 MHz repetition rate in ~20 ps pulses with a FWHM spectral bandwidth down to 2.5 nm, in high beam quality with $M^2$<1.8, with passive power stability as high as 1.3% rms over 2 hours. With further design improvements, substantial enhancements in OPO efficiency, output power, and tunability, and potential for power scaling are also expected. The demonstrated OPO sources combine the widely established, reliable and cost-effective Nd/Yb-doped solid-state and fiber laser technology as the pump source with readily available MgO:PPLN as the nonlinear crystal, thus paving the way for the realization of a new class of practical high-average-power pulsed laser sources for wavelength generation near 2 μm, which will find practical utility for many applications, including pumping of long-wavelengths OPOs into the mid-IR.

**Funding**: Ministro de Ciencia, Innovación y Universidades (MICINN) (nuOPO, TEC2015-68234-R); Generalitat de Catalunya (CERCA Programme); European Commission (EC) (Project Mid-Tech, H2020-MSCA-ITN-2014); Severo Ochoa Programme for Centres of Excellence in R&D and the European Social Fund (BES-2016-079359, Project: SEV-2015-0522-16-1); Fundación Cellex.

**Acknowledgment:** H. Ye acknowledges the support of the Marie Curie Actions: Innovative Training Network through the Mid-Tech project. B. Nandy acknowledges the help and support from K. Devi at several instances.

## REFERENCES


1. P. J. Gilling, C. B. Cass, M. D. Cresswell, A. R. Malcolm, and M. R. Fraundorfer, "The use of the holmium laser in the treatment of benign prostatic hyperplasia," J. Endourol. **10**(5), 459-461 (1996).
2. J. Qin, L. Shi, S. Dziennis, R. Reif, and R. K. Wang, "Fast synchronized dual-wavelength laser speckle imaging system for monitoring hemodynamic changes in a stroke mouse model," Opt. Lett. **37**(19), 4005-4007 (2012).
3. J. Wang, Y. Wang, B. Li, D. Feng, J. Lu, Q. Luo, and P. Li, "Dual-wavelength laser speckle imaging to simultaneously access blood flow, blood volume, and oxygenation using a color CCD camera," Opt. Lett. **38**(18), 3690-3692 (2013).
4. J. L. Machol, R. M. Hardesty, B. J. Rye, and C. J. Grund, "Proposed compact, eye-safe lidar for measuring atmospheric water vapor," In: A. Ansmann et. al. (eds.), Advances in Atmospheric Remote Sensing with Lidar. Springer, 321-324 (1997).
5. S. Cha, K. P. Chan, and D. K. Killinger, "Tunable 2.1-μm Ho lidar for simultaneous range-resolved measurements of atmospheric water vapor and aerosol backscatter profiles," Appl. Opt. **30**(27), 3938-3943 (1991).
6. S. W. Henderson, C. P. Hale, J. R. Magee, M. J. Kavaya, and A. V. Hauffaker, "Eye-safe coherent laser radar system at 2.1 μm using Tm, Ho: YAG lasers," Opt. Lett. **16**(10), 773-775 (1991).
7. S. Ishii, K. Mizutani, H. Fukuoka, T. Ishikawa, B. Philippe, H. Iwai, T. Aoki, T. Itabe, A. Sato, and K. Asai, "Coherent 2 μm differential absorption and wind lidar with conductively cooled laser and two-axis scanning device," Appl. Opt. **49**(10), 1809-1817 (2010).
8. D. Yan, Y. Wang, D. Xu, P. Liu, C. Yan, J. Shi, H. Liu, Y. He, L. Tang, J. Feng, J. Guo, W. Shi, K. Zhong, Y. H. Tsang, and J. Yao, "High-average-power, high-repetition-rate tunable terahertz difference frequency generation with GaSe crystal pumped by 2 μm dual-wavelength intracavity KTP optical parametric oscillator," Photon. Res. **5**(2), 82-87 (2017).
9. F. Wang, D. Shen, D. Fan and Q. Lu, "Widely tunable dual-wavelength operation of a high-power Tm: fiber laser using volume Bragg gratings," Opt. Lett. **35**(14), 2388-2390 (2010).
10. M. R. K. Soltanian, H. Ahmad, A. Khodaie, I. S. Amiri, M. F. Ismail and S. W. Harun, "A stable dual-wavelength Thulium-doped fiber laser at 1.9 μm using photonic crystal fiber," Sci. Rep. **5**, 14537 (2015).
11. L. C. Kong, Z. P. Qin, G. Q. Xie, X. D. Xu, J. Xu, P. Yuan and L. J. Qian, "Dual-wavelength synchronous operation of a mode-locked 2-μm Tm: $CaYAlO_4$ laser," Opt. Lett. **40**(3), 356-358 (2015).
12. M. Henriksson, M. Tiihonen, V. Pasiskevicius, and F. Laurell, "$ZnGeP_2$ parametric oscillator pumped by a linewidth-narrowed parametric 2 μm source," Opt. Lett. 31(12), 1878-1880 (2006).
13. D. Yan, Y. Wang, D. Xu, W. Shi, K. Zhong, P. Liu, C. Yan, J. Mei, J. Shi and J. Yao, "High power, widely tunable dual-wavelength 2 μm laser based on intracavity KTP optical parametric oscillator," J. Phys. D: Appl. Phys. **50**, 035104 (2017).
14. F. Ganikhanov, T. Caughey, and K. L. Vodopyanov, "Narrow-linewidth middle-infrared $ZnGeP_2$ optical parametric oscillator," J. Opt. Soc. Am. B 18(6), 818-822 (2001).
15. K. L. Vodopyanov, O. Levi, P. S. Kuo, T. J. Pinguet, J. S. Harris, and M. M. Fejer, "Optical parametric oscillation in quasi-phase-matched GaAs," Opt. Lett. **29**(16), 1912-1914 (2004).
16. S. Haidar and H. Ito, "Injection-seeded optical parametric oscillator for efficient difference frequency generation in mid-IR," Opt. Commun. **171**(1-3), 171-176 (1999).
17. K. L. Vodopyanov, I. Makasyuk, and P. G. Schunemann, "Grating tunable 4-14 μm GaAs optical parametric oscillator pumped at 3 μm," Opt. Express 22(4), 4131-4136 (2014).
18. L. Maidment, P. G. Schunemann, and D. T. Reid, "Molecular fingerprint-region spectroscopy from 5 to 12 μm using an orientation-patterned gallium phosphide optical parametric oscillator," Opt. Lett. **41**(18), 4261-4264 (2016).
19. H. Huang, H. Wang, and D. Shen, "VBG-locked continuous-wave and passively Q-switched Tm:$Y_2O_3$ ceramic laser at 2.1 μm," Opt. Mat. Express **7**(9), 3147-3154 (2017).
20. A. Hemming, N. Simakov, J. Haub, and A. Carter, "A review of recent progress in holmium-doped silica fibre sources," Opt. Fiber Technol. **20**(6), 621-630 (2014).
21. J. Kwiatkowski, J. K. Jabczynski, W. Zendzian, L. Gorajek, and M. Kaskow, "High repetition rate, Q-switched Ho: YAG laser resonantly pumped by a 20 W linearly polarized Tm: fiber laser," Appl. Phys. B **114**(3), 395-399 (2014).
22. J. Saikawa, M. Fujii, H. Ishizuki, and T. Taira, "52 mJ narrow-bandwidth degenerated optical parametric system with a large-aperture periodically poled MgO: $LiNbO_3$ device," Opt. Lett. **31**(21), 3149-3151 (2006).
23. S. Chaitanya Kumar and M. Ebrahim-Zadeh, "Yb-fiber-based, high-average-power, high-repetition-rate, picosecond source at 2.1 μm," Laser Photonics Rev. **10**(6), 970-977 (2016).
24. P. Schlup, I. T. McKinnie and S. D. Butterworth, "Single-mode, singly resonant, pulsed periodically poled lithium niobate optical parametric oscillator," Appl. Opt. 38(36), 7398-7401 (1999).

25. O. Paul, A. Quosig, T. Bauer, M. Nittmann, J. Bartschke, G. Anstett, and J. A. L'Huillier, "Temperature-dependent Sellmeier equation in the MIR for the extraordinary refractive index of 5% MgO doped congruent LiNbO3," J. Appl. Phys. B. **86**, 111–115 (2007).
26. M. Ebrahim-Zadeh and M. H. Dunn, "Optical parametric oscillators," Handbook of optics, 2nd ed. (Optical Society of America, Washington, D.C.), Chapter 22 (2000).
27. C. Laporte, J. Dherbecourt, J. Melkonian, M. Raybaut, C. Drag, and A. Godard, "Analysis of cavity-length detuning in diffraction-grating narrowed picosecond optical parametric oscillators," J. Opt. Soc. Am. B **31**(8), 1026-1034 (2014).